FREE BOUNDARY VISCOUS FLOWS AT MICRO AND MESOLEVEL DURING LIQUID COMPOSITES MOLDING PROCESS

Zuzana Dimitrovová* and Suresh G. Advani#

*Researcher of IDMEC / Invited Assistant Professor, Department of Mechanical Engineering, ISEL, Portugal

#Professor, Department of Mechanical Engineering and Center for Composite Materials, University of Delaware, USA

ABSTRACT: Numerical simulation aspects related to low Reynolds number free boundary viscous flows at micro and mesolevel during the resin impregnation stage of the Liquid Composite Molding (LCM) Process are presented in this article. Free boundary program (FBP), developed by the authors is used to track the movement of the resin front accurately by accounting for the surface tension effects at the boundary. Issues related to the global and local mass conservation (GMC and LMC) are identified and discussed. Unsuitable conditions for LMC and consequently GMC are uncovered in mesolevel filling at low capillary number, and hence a strategy for the numerical simulation of such flows is suggested.

FBP encompasses a set of subroutines that are linked to modules in ANSYS. FBP can also capture the void formation dynamics based on the analysis developed. We present resin impregnation dynamics in two dimensions. Extension to three dimensions is a subject for further research. Several examples of stabilization validation techniques are compared.

KEYWORDS: resin transfer molding, liquid composite molding, free boundary flows, microlevel analysis, mesolevel analysis

INTRODUCTION

Liquid Composite Molding (LCM) is a class of processes in which the fiber preform is held stationary in the mold and a thermoset resin is injected into the mold to cover the empty spaces between the fibers. LCM processes such as Resin Transfer Molding (RTM) and Vacuum Assisted Resin Transfer Molding (VARTM) are widely used processes to manufacture advanced composites with continuous fiber reinforcements. RTM filling phase consists of injection of a thermoset resin into a closed and clamped mould with a pre-placed fiber preform and main objectives of the related fluid flow analysis are free boundary progression and pressure determination. When injection is completed, the mould temperature is increased to activate the resin reaction, the liquid resin cures and solidifies and the part is demolded. From manufacturing viewpoint, one would like to fill the spaces between the fibers before it initiates the curing process, because the viscosity of the resin increases rapidly with degree of cure and high viscosity might aggravate or even stop resin flow leaving voids and dry spots, which are detrimental for the mechanical performance of the final part [1].

Fiber preforms composed by knitted layers from fiber tows, allow one to tailor better mechanical properties of final composites and facilitated arrangement of the reinforcement in the mold cavity. On the other hand, this type of fiber preform is composed of not single but dual porous media and therefore can cause very high non-uniformity in the resin progression, not only across the thickness, but also in the plane of fabricated components [2-5]. Thus, the resin impregnation stage consists of many phenomena, which are known to occur in RTM applications, but are still not well understood neither experimentally nor theoretically.

Resin impregnation or infiltration is usually modeled as a liquid flowing though a porous medium and assumptions of sharp bulk flow front and quasi steady state process are generally adopted for the macrolevel filling. Therefore Darcy's law, as an exact homogenization result for macrolevel analysis when incompressible Newtonian resin slowly flows at microlevel [6-7] is commonly used in numerical simulation codes. Fixed mesh algorithms are more common than moving mesh ones and new flow front is determined by CV/FEM ([8]), CE/FEM ([9-10]) or VOF ([11]) method. Liquid advance can also be achieved by introduction of a new variable, saturation s, which modifies the continuity equation into [12]:

$$\phi \frac{\partial s}{\partial t} = -\nabla \cdot \mathbf{v}^{D}, \qquad (1)$$

and allows to capture partially saturated transition region formed along the macroscopic boundary or in the neighborhood of dry spots (regions devoid of resin). In Eq. (1), ϕ is the porosity of the fiber preform, t is the time, ∇ stands for spatial gradient and Darcy's velocity $\mathbf{v}^D=\langle\mathbf{v}\rangle$ is the phase averaged velocity related to the intrinsic phase average by $\mathbf{v}^D = \phi\langle\mathbf{v}\rangle^f$, where $\mathbf{v}$ is local velocity vector. These definitions were established originally for saturated flows. Although Eq. (1) is adopted by several authors, Darcy's law is rarely modified in the way to satisfy Eq. (1) exactly. The definition of $\mathbf{v}^D$ for saturated flows is unclear in partially saturated regions. Moreover, effective (instead of absolute $\mathbf{K}$) permeability tensor $\mathbf{K}^{ef}$ should be used, because the flow is not yet stabilized in the transition region and surface tension influence represented by homogenized capillary pressure can be important at the flow front region. In summary, two more functions, relative permeability k(s) and macroscopic capillary pressure $P_c(s)$, both being functions of saturation, must enter into the analysis [13-14] and modify Darcy's law into:

$$\mathbf{v}^{D}(s) = -\frac{k(s)}{\mu}\mathbf{K} \cdot \nabla\big(P(s) - P_c(s)\big), \qquad (2)$$

where μ is resin viscosity, effective permeability $\mathbf{K}^{ef}(s)=k(s)\cdot\mathbf{K}$ (in anisotropic case it is better to use $K_{ij}^{ef} = k_{ij}(s)\cdot K_{ij}$, $k_{ij} \in [0,1]$, $k_{ij}(0)=0$ and $k_{ij}(1)=1$) and P is the intrinsic phase average of the local pressure $P = \langle p\rangle^f$. This definition was originally also established for saturated flows. Homogenized capillary pressure $P_c(s)$ is a macroscopic analogue of the microscopic p_c, it obeys $P_c(1)=0$ and unlike p_c, it acts in the full transition region without being dependent on the actual "front curvature". Its definition can be set as $P_c = 2\gamma\langle H\rangle$, where H is the mean curvature and γ is the resin surface tension. In order to apply gradient in Eq. (2) also functional dependence of saturation on spatial variable $\mathbf{x}$ must be known. Eqs. (1-2) reduce to the steady-state formulation in the fully saturated region.

$P_c(s)$ and k(s) must enter macroscopic analysis as known data; therefore they must be determined elsewhere, experimentally or by exploiting homogenization techniques applied to resin progression results from micro and/or mesolevel. [15] with experimental values adopted from other fields of research for $P_c(s)$ and k(s) were used in the first attempts of implementation of Eq. (2) in the RTM process. Our objective is to develop the numerical simulation that will model with sufficient accuracy resin progression at the micro and mesolevel and allow consequently developing methodologies for determination of relative permeability and macroscopic capillary pressure by homogenization techniques. Additional benefits from such formulation are that one can determine the requirements on resin properties and process conditions for favorable filling without the dangers of void formation. Also one can detect possible filling anomaly that originates at the microlevel and cannot be represented at the macrolevel filling simulation with macroscopic variables. FBP results have been published for microlevel filling along with first methodologies for relative permeability and homogenized capillary pressure determination under some restrictions in [16]. For the time being FBP can handle mesolevel filling, its efficiency of calculation was improved by inclusion of several stabilization techniques, improving not only the speed of calculation but also the accuracy of calculations. Discussion of numerical aspects related to these issues is the aim of this paper.

Not much work has been done so far in modeling of free boundary viscous flows at the micro and especially at the mesolevel for the RTM manufacturing process. Many simulations available nowadays in other fields of research are not applicable here. Only simulations by Lattice Boltzman method [17] can handle transient mesolevel filling and require a very different approach.

MICROLEVEL ANALYSIS

Resins especially developed for RTM processes usually belong to the group of incompressible Newtonian liquids, corresponding flow has low Reynolds number and by adopting the common restriction to quasi steady state process, one must solve Stokes problem [18] in the currently filled domain Ω_{t_k} at each discretized time t_k:

$$\nabla \cdot \mathbf{v} = 0 \text{ and } \nabla p = \mu \Delta \mathbf{v} \quad \text{in } \Omega_{t_k} \quad \forall k, \tag{3}$$

When fibers are rigid, impermeable and with fixed location during injection, the following boundary conditions, under a usual omission of air pressure, must be fulfilled:

$$\text{at the resin front: } \boldsymbol{\tau}^v \cdot \mathbf{n} = \mathbf{0},\ \boldsymbol{\sigma} \cdot \mathbf{n} = -p_c \mathbf{n} = -2\gamma H \mathbf{n} \quad \text{at } \Gamma^r_{t_k}, \tag{4a}$$

$$\text{at the fiber boundary: } \mathbf{v} = \mathbf{0} \quad \text{at } \Gamma^f_{t_k}, \tag{4b}$$

$$\text{at the inlet: } \mathbf{v} = \mathbf{v}_0 \text{ or } p = p_0 \quad \text{at } \Gamma^{in}_{t_k}, \tag{4c}$$

where $\boldsymbol{\tau}^v$ is viscous shear stress and $\boldsymbol{\sigma}$ is stress tensor. $\mathbf{v}_0$ and p_0 stand for given imposed values. Besides Eq. (4), contact angle must be formed at the resin front-fiber contact point ($\Gamma^r_{t_k} \cap \Gamma^f_{t_k}$). Additional condition to move the resin front yields from free surface equation, [18-19]:

$$\frac{Df}{Dt} = \frac{\partial f}{\partial t} + \mathbf{v} \cdot \nabla f = 0 \quad \text{at } \Gamma^r_{t_k}, \tag{5}$$

where implicit function $f(\mathbf{x}(t),t)=0$ describes the moving front and $\mathbf{x}$ is spatial variable.

FBP is concerned with the moving flow front, which requires results extraction for a current time t_k, determination of new resin front position $\Gamma^r_{t_{k+1}}$ at t_{k+1}, stabilization of this new front, application and stabilization of boundary conditions at $\Gamma^r_{t_{k+1}}$ according to Eq. (4a), application of other boundary conditions stated in Eq. (4b-c) and adjustment into contact angle if required. Then the base analysis is solved by ANSYS FLOTRAN module and the process is repeated.

To describe the details, one must first, at each frontal point at a current time, t_k, extract local velocities and create a local coordinate system close to it, where the flow front is locally approximated by a smooth circular or elliptical curve, which includes two adjacent points. This permits one to define uniquely the outer normal vector to the flow front. Next, a second local coordinate system is created with axes aligned to the tangential, x_t, and the outer normal vector, x_n. The flow front is described locally by $x_n = g(x_t)$ with respect to this coordinate system, which modifies Eq. (5) into:

$$v_n - v_t \frac{\partial g}{\partial x_t} = v_n = \frac{\partial g}{\partial t} \text{ (since } \frac{\partial g}{\partial x_t} = 0\text{)}. \tag{6}$$

Then the point new position is determined as:

$$x_{n,t_{k+1}} = x_{n,t_k} + \Delta x_{n,t_k} = x_{n,t_k} + \Delta t_k \cdot v_{n,t_{k+\alpha}} = x_{n,t_k} + \left(t_{k+1} - t_k\right) v_{n,t_{k+\alpha}} \text{ and} \tag{7a}$$

$$x_{t,t_{k+1}} = x_{t,t_k}, \tag{7b}$$

where parameter $\alpha \in [0,1]$ will be specified later on. The smooth curve approximation as described above is repeated, now for the new front $\Gamma^r_{t_{k+1}}$, and the surface curvature is determined in order to calculate the capillary pressure, which is then applied according to Eq. (4a) as piece-wise linear at each frontal line. Finally, other boundary conditions are applied and Stokes problem is solved for in the new domain $\Omega_{t_{k+1}}$.

In FBP there is no need for special treatment of the singularity point at the resin front-fibre contact $\Gamma^r_{t_k} \cap \Gamma^f_{t_k}$. In the case of neglected contact angle formation, resin progression along the fibre surface is ensured by the neighbouring point motion from $\Gamma^r_{t_k}$ (Fig. 1a). If contact angle is formed, in FBP additional circular surface is created (Fig. 1b) in order to adjust exactly to the given angle. Correct determination of the additional circle localization is determined by Maple module.

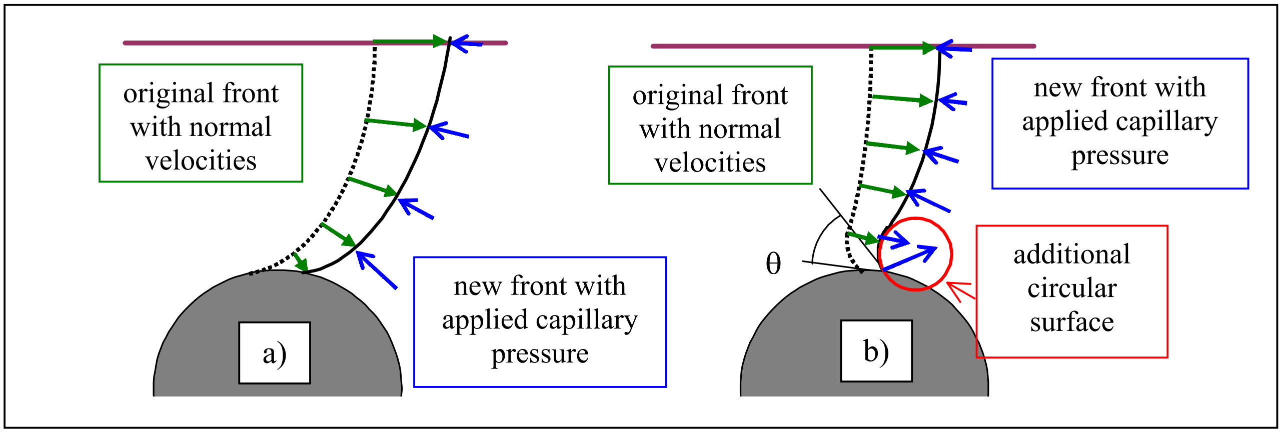

Fig. 1: Front progression along fiber surface: (a) without and (b) with the influence of the contact angle θ formation

As shown in [16], free boundary progression pattern in the same geometry is only dependent on capillary number N_c, defined as $v\mu/\gamma$, where v is a characteristic velocity components of the current case study. When capillary number is low, resin front approaches constant curvature surface and generally low capillary number creates more favorable conditions for injection in view of air entrapment. A negative effect of low capillary number in view of numerical simulation is that the resin front is more sensitive to the time step magnitude and unphysical non-smoothness are more probable to occur. Resin front $\Gamma^r_{t_k}$ can start to oscillate due to these factors, as it is explained in Fig. 2. If the time step is doubled (Fig. 2b) than it is acceptable (Fig. 2a), curvature of the new front $\Gamma^r_{t_{k+1}}$ can be unrealistically reversed creating high capillary pressure in opposite direction, which will push the front more than necessary against the flow direction. This will create in the next step high capillary pressure acting in the flow direction, pulling the front more than necessary in the flow direction and this process will lead to oscillations and instability. For better control, a maximum normal advance is used to calculate the actual time step Δt_k.

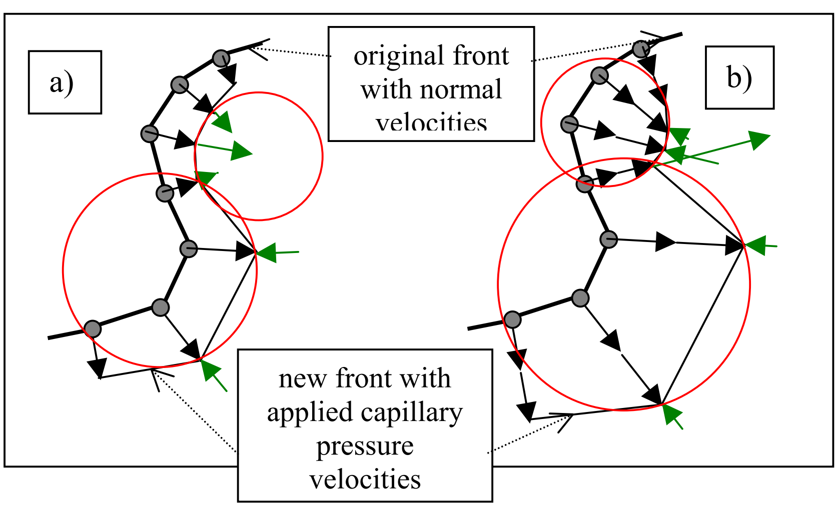

Fig. 2: Onset of front oscillation due to an inadequate time step

Two following stabilization techniques are implemented in FBP in order to decrease the danger of front oscillations, which can originate due to unphysical non-smoothness, as a result of LMC violation. The first one is based on parameter α, introduced in Eq. (7) as $\Delta x_{n,t_k} = \Delta t_k \cdot v_{n,t_{k+\alpha}}$. In fully explicit approach α=0, however, more correctly it might be assumed that:

$$v_{n,t_{k+\alpha}} = \left(v_{n,t_k} + v_{n,t_{k+1}}\right)/2 = \left(v_{n,t_k} + \beta_{n,t_k} v_{n,t_k}\right)/2 = v_{n,t_k}\left(1+\beta_{n,t_k}\right)/2\,, \tag{8}$$

where parameter β_{n,t_k} can be calculated from LMC in the form:

$$R_{n,t_k} v_{n,t_k} = \left(R_{n,t_k} + \Delta x_{n,t_k}\right) v_{n,t_{k+1}} = \beta_{n,t_k}\left(R_{n,t_k} + \Delta x_{n,t_k}\right) v_{n,t_k}\,, \tag{9}$$

where R_{n,t_k} is curvature radius of the free front at the location under consideration. This procedure maintains better LMC especially in curved regions, as it can be seen in Fig. 3. An iterative algorithm according to Eqs. (8-9) is included in FBP, where in the first iteration radius R_{n,t_k} from smooth curve approximation is implemented, while in consequent iterations areas formed by straight lines are used to update β_{n,t_k}. Number of consequent iterations can be equal to 0 in the case of fully explicit approach, i.e. when α=0 and β_{n,t_k}=1 $\forall$n.

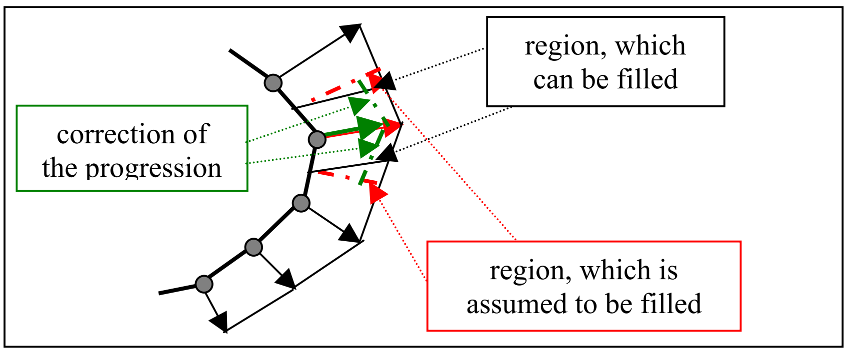

Fig. 3: Stabilization technique of LMC in significantly curved fronts

The other stabilization algorithm of unphysical non-smoothness is explained in Fig. 4. When a "sharp" angle on the flow front (concept of this sharpness is determined by user specified value) is detected, the new position $x_{n,t_{k+1}}$ is moved to the location in the middle of the normal line to the original front $\Gamma^r_{t_k}$ correcting intersection with a straight line between two neighbouring new points $x_{n+1,t_{k+1}}$ and $x_{n-1,t_{k+1}}$ and the sharp location. Also this algorithm is introduced in an iterative way.

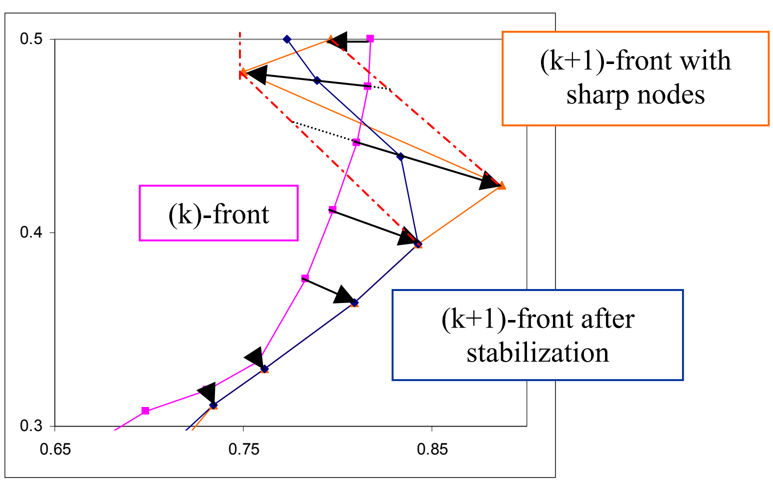

Fig. 4: Stabilization technique of unphysical non smoothness

It can be remarked that for microlevel problems neither of these two stabilization techniques were really necessary, their demand was originated in mesolevel analysis. As already pointed out, FBP concerns only with the moving flow front, therefore ANSYS FLOTRAN capabilities can be fully explored in each base analysis, including non-Newtonian resin behavior, coupling with heat transfer analysis and/or fibers deformation due to the resin passage. Adaptive h-method or other techniques for precision improvement with less computational time can also be implemented automatically.

MESOLEVEL ANALYSIS

In mesolevel analysis liquid flowing along two different levels have to be combined together at each discretized time t_k, which implies that Stokes problem in inter-tow spaces $\Omega_{t_k}^{S_r}$ and Darcy's problem in intra-tow region $\Omega_{t_k}^{B_r}$ have to be solved. In fact, Darcy's law must be modified to Brinkman equations, in order to account for viscous stress at the interface between these two regions ($\Gamma_{t_k}^{S_r - B_r}$):

$$\text{in inter-tow spaces: } \nabla \cdot \mathbf{v} = 0 \text{ and } \nabla p = \mu \Delta \mathbf{v} \quad \text{in } \Omega_{t_k}^{S_r} \quad \forall k \tag{10a}$$

(Stokes equations),

$$\text{in intra-tow spaces: } \nabla \cdot \langle \mathbf{v} \rangle = 0 \text{ and } \nabla \langle p \rangle^{f} = \mu \Delta \langle \mathbf{v} \rangle - \mu \mathbf{K}^{-1} \langle \mathbf{v} \rangle \quad \Omega_{t_k}^{B_r} \quad \forall k \tag{10b}$$

(Brinkman equations).

ANSYS FLOTRAN can account for porous media influence by introduction of distributed resistance. Averaged values in Eq. (10) are therefore important mainly from theoretical point of view, while numerically both velocity and pressure maintain their meaning as nodal variable in both regions, preserving all necessary continuity requirements at $\Gamma_{t_k}^{S_r - B_r}$.

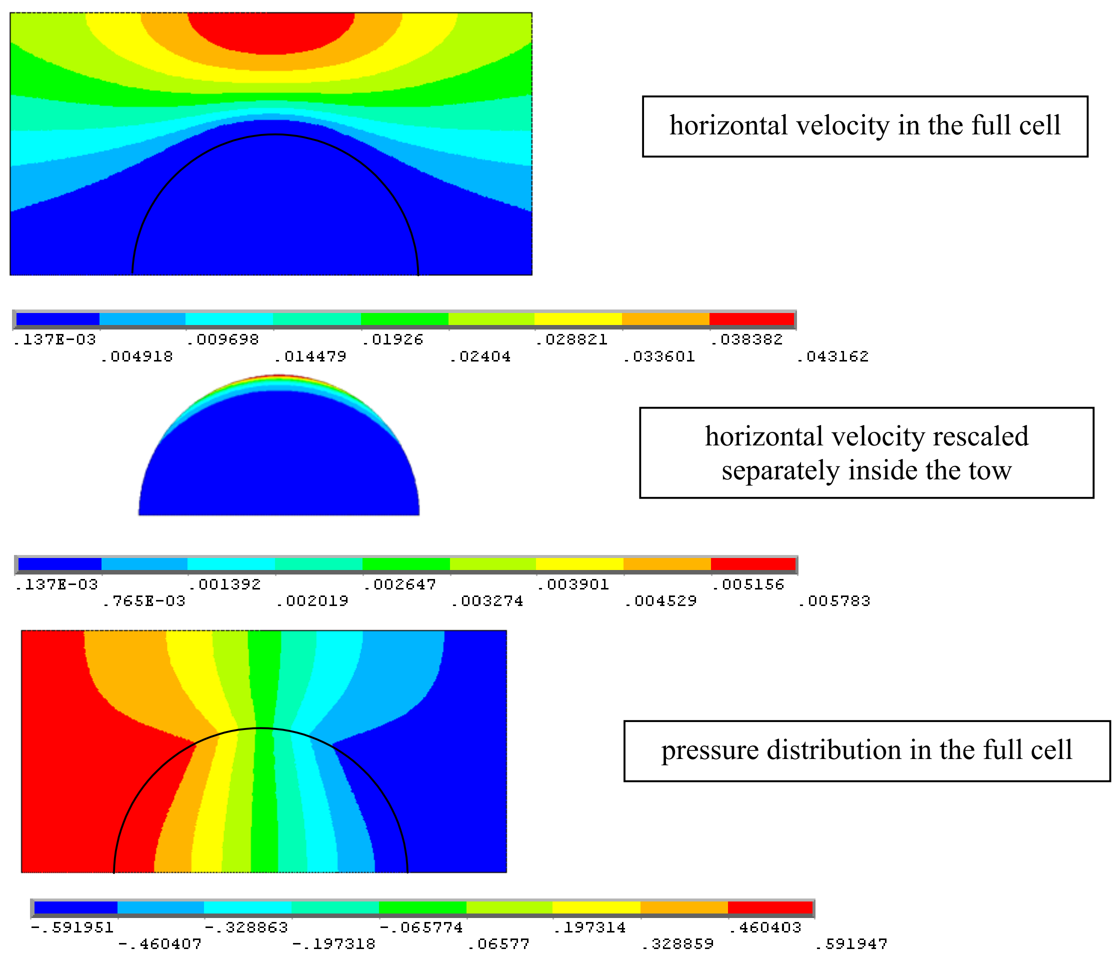

Fig. 5: Dimensionless velocity and pressure distribution in the saturated basic cell related to calculation of the homogenized permeability

First of all, the problem of homogenized permeability calculation, verifying the distributed resistance introduction, is presented. Particularly, flow across square arrangement of cylindrical fiber tows with circular cross section of relative radius 0.3 and intra-tow porosity ϕ_t=0.9 is considered. Let each tow contains 89 fibers of relative diameter 0.02 with square arrangement, yielding intra-tow permeability of $1{,}28\cdot 10^{-4}$ unit^2. According to homogenization techniques permeability equals to averaged velocity when a unit macroscopic pressure gradient is imposed on a saturated basic cell containing a unit viscosity liquid. Periodicity of liquid velocity and anti-periodicity of local pressure are applied at the inlet/outlet fronts and symmetry/anti-symmetry conditions are required on the others boundaries. Results are shown in Fig. 5, velocity and pressure distribution are in agreement with expected and published results [20-21]. Dimensionless homogenized permeability is determined as 0.0131, which corresponds to the 19% increase against 0.011 of permeability of the same geometry with "impermeable tow". It should be remarked in this context, that homogenized permeability cannot depend only on ϕ_t, because dimensional factor is always important. Numerical simulation results are dependent on the "dimensional" intra-tow permeability. The same value of $1{,}28\cdot 10^{-4}$ unit^2 could be achieved e.g. for ϕ_t=0.6 and 10 fibers of relative diameter 0.12.

In order to verify correctness of the results, LMC error was also calculated and verified. The absolute value for the total fluid flux entering and exiting each FE, should be zero. The relative LMC error switches the absolute value into dimensionless number by dividing it by square root of the FE area and by the maximum velocity component related to this element. In this example both absolute and relative LMC error are concentrated at the inlet/outlet boundaries, only in relative values there is slight increase along the tow outer surface, but not significant. Therefore distributed resistance introduction fits well to our problems.

When both domains $\Omega_{t_k}^{S_r}$ and $\Omega_{t_k}^{B_r}$ are included in numerical simulation, one has to be careful with the interpretation of the free boundary condition (Eq. (5) at microlevel) and capillary pressure application (Eq. (4a) at microlevel). Free boundary condition will have different formulation in fiber tows as follows:

$$\frac{\partial f}{\partial t} + \mathbf{v}\cdot\nabla f = 0 \qquad \text{at } \Gamma_{t_k}^{S_r}, \tag{11a}$$

$$\frac{\partial f}{\partial t} + \frac{1}{\phi_t}\langle \mathbf{v}\rangle\cdot\nabla f = 0 \qquad \text{at } \Gamma_{t_k}^{B_r}, \tag{11b}$$

where $\Gamma_{t_k}^{S_r}$ and $\Gamma_{t_k}^{B_r}$ are parts of the free boundary contained in the Stokes and Brinkman region, respectively, and ϕ_t is intra-tow porosity. Consequently, velocities extracted in intra-tow spaces for the new front determination $\Gamma_{t_{k+1}}^{B_r}$ must be corrected by a factor $1/\phi_t$.

Regarding the capillary pressure application, it holds:

$$\boldsymbol{\sigma}\cdot\mathbf{n} = -p_c\mathbf{n} = -2\gamma H\mathbf{n} \qquad \text{at } \Gamma_{t_k}^{S_r}, \tag{12a}$$

$$\langle\boldsymbol{\sigma}\rangle^f\cdot\mathbf{n} = -P_c\mathbf{n} = -2\gamma\langle H\rangle\mathbf{n} \qquad \text{at } \Gamma_{t_k}^{B_r}. \tag{12b}$$

Fiber tows in mesolevel analysis belong to single porous medium with uniform pore size, therefore transition region can be omitted and the homogenized value P_c can be calculated as explained in [16].

From the other boundary conditions only Eq. (4c) comes into account and it is unchanged, when applied at Stokes boundary. Now first problems in numerical simulation of the mesolevel analysis are clearly visible and are related to the node at the intersection $\Gamma_{t_k}^{S_r}\cap\Gamma_{t_k}^{B_r}\cap\Gamma_{t_k}^{S_r-B_r}$, which we will name as the transition node. The problems are:

- application of Eq. (11) is ambiguous at the transition node;
- application of Eq. (12) is ambiguous at the transition node.

In order to eliminate this ambiguity, FE mesh around the transition node is refined, condition from Eq. (12) is not applied, it is imposed in the way as it should be only at proximal frontal nodes; and automatic correction of the free front to straight line using two neighboring new nodal positions, as it is shown in Fig. 6, is implemented.

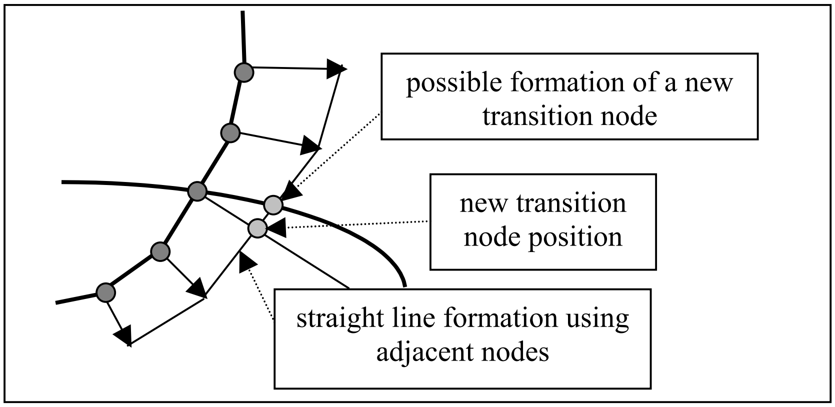

Fig. 6: Treatment of the free boundary advance at the transition node

Such treatment of the transition node and stabilization techniques described in the previous section can ensure correct results of free front boundary pattern and GMC for relatively high capillary numbers. In the case of very low capillary numbers, alternative strategies are suggested and verified in the following example: Cylindrical fiber tows have elliptical cross section with principal semi-axes 0.8mm and 0.35mm, their arrangement is rectangular with distances between centers 2mm and 1mm in horizontal and vertical direction, respectively. Resin is injected at the left hand side of the specimen with constant uniformly distributed velocity v_0=1mm/s along the height h=0.5mm. Only the part shown in Fig. 7 can be studied due to symmetry. Resin properties are: viscosity μ=0.05 Pa·s and surface tension γ=0.02N/m, yielding the capillary number as 0.0025. Intra-tow porosity is 0.4, giving the total porosity of 0.736. Fibers diameter is chosen as 14.67μm implying $K=1.6\cdot10^{-7}$ mm^2. According to [16], for contact angle of 0º medium capillary force calculated analytically is $1.57\ 10^{-5}$N/mm, therefore P_c can be estimated as 1.9kPa.

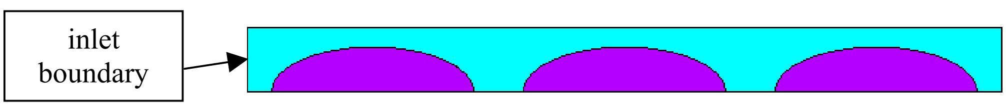

Fig. 7: Geometrical specification of the studied example

Two alternative strategies were examined:

- *Correction analysis:* when analogy with incompressible elasticity is used for Stokes flow, results are always reliable and no error concentration around the free front is detected. There is no such simple analogy for mesolevel analysis, but at least velocities or pressures at the interface $\Gamma_{t_k}^{S_r-B_r}$ might be extracted from original FLOTRAN analysis and additional structural analysis can be performed, to recalculate velocities distribution.
- *Smooth analysis:* capillary pressure to be applied at $\Gamma_{t_k}^{S_r}$ is stabilized before the application; least square approximation in Maple module by constant or linear function can be used.

As GMC verification, area of the total injected resin from infiltrations by Correction analysis is compared to analytical ($v_0\cdot h\cdot t=0.5t$) and original analysis values in Fig. 8. Numerically the total injected resin is calculated at each t_k as $A^S+\phi_t\cdot A^B$, where A^S and A^B is the total area of FEs in Stokes and Brinkman region, respectively. It is seen that Correction analysis with extracted velocities at $\Gamma_{t_k}^{S_r-B_r}$ acceptably approaches the analytical value even for quite rough FE meshes. Much better results were obtained in Smooth analysis, for both linear and constant approximation of the capillary pressure in Stokes region. In Fig. 9 there is noticeable drop in the total resin area in early time steps, but this error maintains its magnitude and does not increase along filling time as in the Correction analysis.

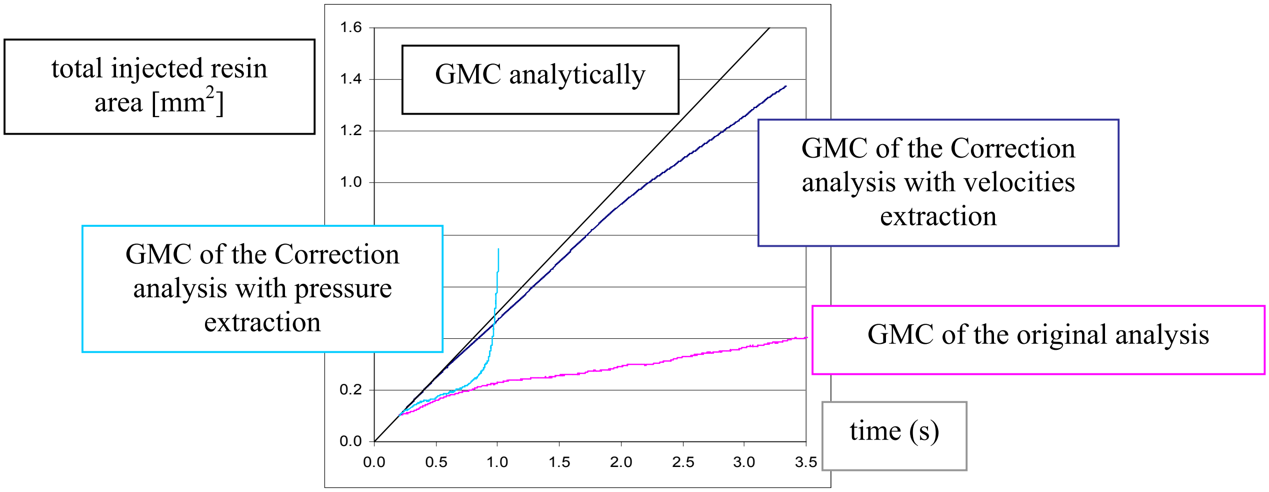

Fig. 8: CGM of the Correction analysis compared to the analytical value and the original analysis

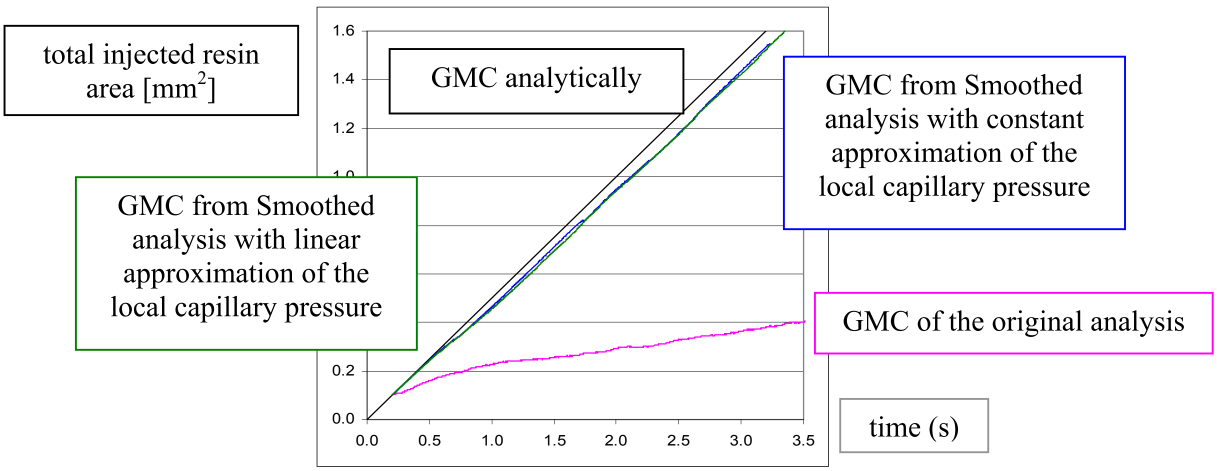

Fig. 9: CGM of the Smooth analysis compared to the analytical value and the original analysis

Free front pattern is shown in Fig. 10 in Correction analysis with velocity extraction and Smooth analysis with constant capillary pressure approximation, in which free fronts are more evenly spaced.

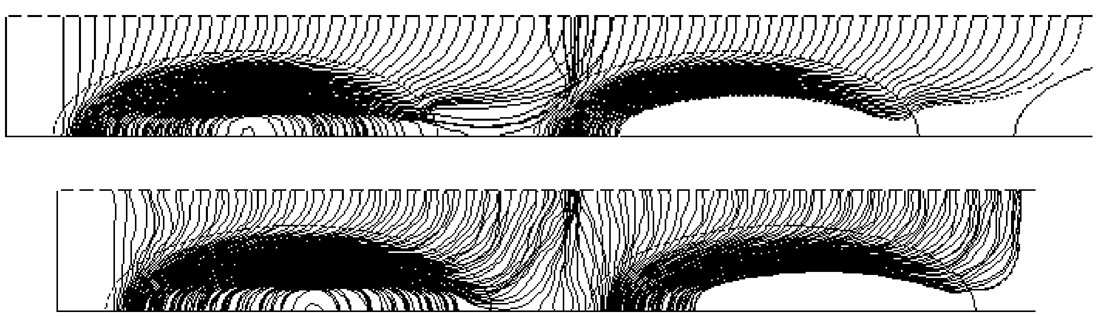

Fig. 10: Free front pattern from the Smooth analysis (above) and the Correction analysis (below)

SUMMARY

In this article free boundary progression pattern at micro and mesolevel filling of RTM manufacturing process determined by FBP was discussed. FBP is a Free Boundary Program that integrates routines and interconnecting moduli written in Ansys Parametric Design Language (APDL), FORTRAN and

Maple, applied directly to FLOTRAN CFD ANSYS module to resolve a base analysis. Currently only two dimensional problems can be treated; extension to three dimensions is a subject for further research. Stabilization techniques described in this article were mainly introduced because of the LMC error concentrated along the free boundary inside the Stokes region and are only necessary for low capillary number sensitive to infiltrations at mesolevel. No problems were detected at the interface $\Gamma_{t_k}^{S_r-B_r}$, although treated by FE and not by CV/FEM or VOF or with the help of Lattice Boltzman method. FBP belongs to the group of moving mesh algorithms and has the potential to calculate several characteristics averages to be used in homogenization procedures.

REFERENCES

[1] Advani, S.G., Bruschke, M.V., Parnas, R.S., Resin transfer molding, in *Flow and Rheology in Polymeric Composites Manufacturing*, Ed. S.G. Advani, Elsevier Publishers, Amsterdam, pp. 465-516, 1994.

[2] Parnas, R.S., Phelan, F.R., "The effect of heterogeneous porous media on mold filling in resin transfer molding", *SAMPE Quarterly*, **22**, pp. 53-60, 1991.

[3] Parnas, R.S., Salem, A.J., Sadiq, T.A.K., Wang, H.P., Advani, S.G., "The interaction between micro- and macroscopic flow in RTM preforms", *Composite Structures*, **27**, pp. 93-107, 1994.

[4] Patel, N., Lee, L.J., "Effects of fiber mat architecture on void formation and removal in liquid composite molding", *Polymer Composites*, **16**, pp. 386-399, 1995.

[5] Patel, N., Rohatgi, V., Lee, L.J., "Micro scale flow behavior and void formation mechanism during impregnation through a unidirectional stitched fiberglass mat", *Polymer Engineering and Science*, **35**, pp. 837-851, 1995.

[6] Sanchez-Palencia, E, Non-Homogeneous Media and Vibration Theory, *Lecture Notes in Physics*, 127, Springer-Verlag, pp.129-157, 1980.

[7] Ene, H.I., Polisevski, D., *Thermal Flow in Porous Media*, D. Reidel Publishing Company, 1987.

[8] Bruschke, M.V., Advani, S.G., "A finite element/control volume approach to mold filling in anisotropic porous media", *Polymer Composites*, **11**, pp. 291-304, 1990.

[9] Bruschke, M.V., Advani, S.G., "A numerical approach to model non-isothermal, viscous flow with free surfaces through fibrous media", *International Journal of Numerical Methods in Fluids*, **19**, pp. 575-603, 1994.

[10] Cloete, T.J., van der Westhuizen, J., "An alternative approach to volume flux prediction during FEM modeling of RTM", Proceedings of the 1st South African Conference on Applied Mechanics, July, Midrand, South-Africa, pp. 53-60, 1996.

[11] Hirt, C.W., Nichols, B.D., "Volume of fluid (VOF) method for the dynamics of free boundaries", *Journal of Computational Physics*, **39**, 201-225, 1981.

[12] Lin, M., Hahn, H.T., Huh, H., "A finite element simulation of resin transfer molding based on partial nodal saturation and implicit time integration", *Composites A*, **29A**, pp. 189-198, 1998.

[13] Muskat, M., *The flow of Homogeneous Fluids through Porous Media*, New York, NY:McGraw Hill, (1937).

[14] Collins, R.E., *Flow of Fluids through Porous Media*, Reinhold Publishing Corporation, 1961.

[15] Han, K., *Analysis of Dry Spot Formation and Changes in Liquid Composite Molding,* Ph.D. theses, The Ohio State University, 1994.

[16] Dimitrovová, Z., Advani, S.G., "Analysis and Characterization of Relative Permeability and Capillary Pressure for Free Surface Flow of a Viscous Fluid across an Array of Aligned Cylindrical Fibers", *Journal of Colloid and Interface Science*, **245**, pp. 325-337, 2002.

[17] Spaid, M.A.A., Phelan, F.R., "Modeling void formation dynamics in fibrous porous media with the Lattice Boltzman method", *Composites A*, **29A**, pp. 749-755, 1998.

[18] White, F.M., *Fluid Mechanics*, McGraw-Hill, 1994.

[19] Whitham, G.B., *Linear and Nonlinear Waves*, John Wiley & Sons, New York, 1974.

[20] Ranganathan, S., Phelan, F.R., Advani, S.G., "A generalized model for the transverse fluid permeability in unidirectional fibrous media", *Polymer Composites*, **17**, pp. 222-230, 1996.

[21] Papathanasiou, T.D., "A structure oriented micromechanical model for viscous flow through square arrays of fibre clusters", *Composites Science and Technology*, **56**, pp. 1055-1069, 1996.